3.11. Cracked Section Properties of the Pier Cap Beam

The cracked section properties of the pier cap beam, i.e. I_{exx} and I_{eyy}, can be obtained by using two methods, the moment-curvature method [Priestley and others, 1996] and ACI Equation [*Building,* 2001]. The moment-curvature relationship uses the following equation:

$$EI_e = \frac{M_y}{\phi_y}$$

M_y = the yield moment in the moment-curvature relationship for the cross section

ϕ_y = the yield curvature in the moment-curvature relationship for the cross section

The cracked section properties using this method produced $I_e = 0.17\ I_g$. The complete calculation for this method is presented in Appendix V.

The method using ACI Equation revealed that the pier cap beam was not expected to be cracked at service load level, since $M_{cr} > M_a$ (the maximum positive or negative moment in the pier cap beam) and therefore $I_e = I_g$.

Despite the discrepancy between the result of the moment-curvature method and the ACI Equation, the moment-curvature result was used.

3.12. Section Properties of the Superstructure

A RISA 3D analysis was run in order to investigate whether or not the superstructure was actually cracked during a maximum considered earthquake. An 82-N/mm uniformly distributed load, which was the equivalent earthquake force obtained using the uniform load method that will be explained later in section 3.15.1, was applied along the superstructure. The results showed that the superstructure was not cracked. Therefore the superstructure's gross section properties were used for this bridge. The calculations for this analysis are provided in Appendix XXIV.

3.13. Period of Vibration

After obtaining the cracked section properties for the pier cap beam and the columns, the RISA 3D model of the bridge was modified by changing the gross section properties to the cracked section properties. The next step was to compute the period of vibration of the bridge. There are two methods used to calculate the period of vibration, the uniform load method and the single mode spectral analysis method [MCEER/ATC, 2002].

3.13.1. Uniform Load Method

The uniform load method is basically an equivalent static method of analysis which uses a uniform lateral load to approximate the effect of seismic loads. The method is suitable for common bridges that respond primarily in their fundamental mode of vibration. The complete calculation of the period of vibration of this bridge using the uniform load method is presented in Appendix VI.

The first step of this method was to apply a uniformly unit distributed load p_o, which can be set arbitrarily to any magnitude according to one's preference, over the length of the bridge. For this bridge analysis, p_o was set to 100 N/mm so that the resulting deflections would have a reasonable magnitude. For this bridge, p_o was applied only in the transverse direction. Since the bridge has integral abutments, it was assumed that the bridge superstructure and substructure would move together in an earthquake in the longitudinal direction. Each span of the bridge was divided into sections, eleven in this case, and the lateral displacement of each section was called $v_s(x)$. The bridge lateral loading is shown in Figure 3.13.

The bridge's lateral stiffness (K) and total weight (W) were calculated by using equations 3-1 and 3-2, respectively.

$$K = \frac{p_o L}{v_{s,MAX}} \tag{3-1}$$

L = total length of the bridge

$v_{s,MAX}$ = maximum value of $v_s(x)$

K = 3,070,000 N/mm

$$W = \int w(x)dx \tag{3-2}$$

$w(x)$ = weight per unit length of the dead load of the bridge superstructure and tributary substructure

W = 21,700,000 N

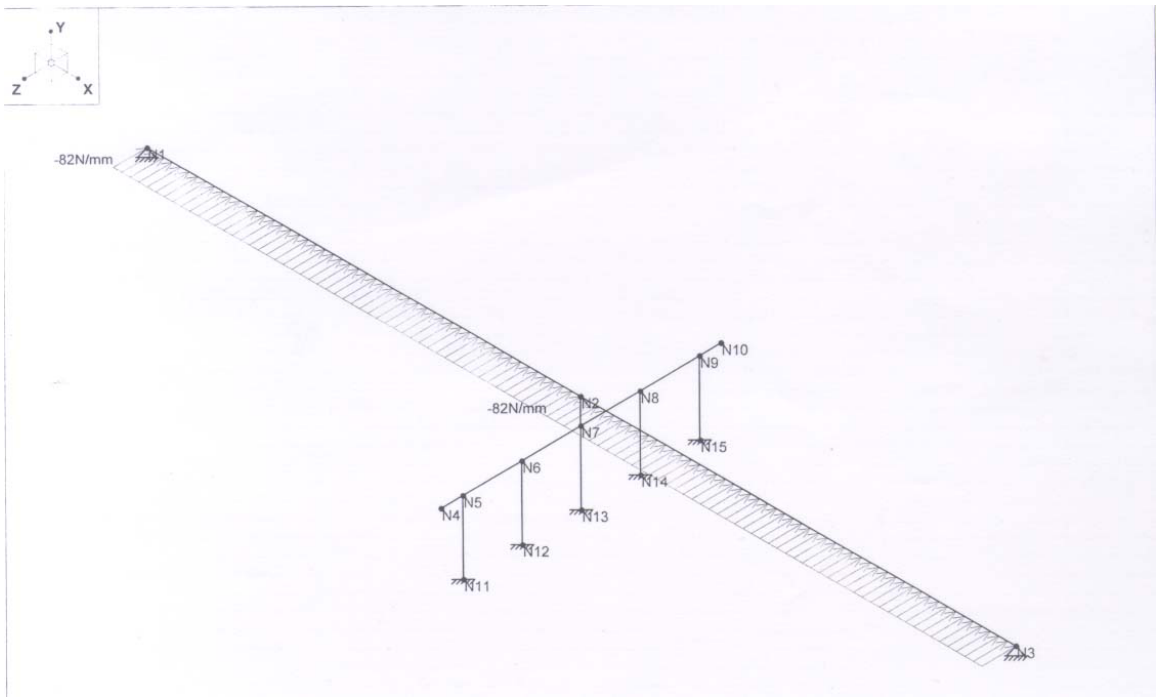

Figure 3.13. The uniform lateral loading on the bridge.

The fundamental period of vibration was calculated using equation (3-3):

$$T = 2\pi\sqrt{\frac{W}{gK}} \tag{3-3}$$

g = acceleration of gravity = 9810 mm/sec^2

T = 0.169 sec.

[MCEER/ATC, 2002].

3.13.2. Single Mode Spectral Analysis Method

The primary difference between this method and the uniform load method is that the equivalent lateral earthquake forces for this method are not uniformly distributed loads over the length of the bridge. Instead, they are of variable magnitude over the length of the bridge, as explained later in section 3.15.2. The complete calculation of the period of vibration using the single mode spectral analysis method is presented in Appendix VII.

As in the uniform load method, first the bridge was subjected to a uniform load p_o of 100 N/mm, and the resulting deflection of each of the eleven sections as given by RISA 3D was called $v_s(x)$. Then the α, β, and γ factors were calculated as follows:

$$\alpha = \int v_s(x)dx \tag{3-4}$$

$$\beta = \int w(x)v_s(x)dx \tag{3-5}$$

$$\gamma = \int w(x)v_s(x)^2 dx \tag{3-6}$$

w(x) = the weight per length of the dead load of the bridge superstructure and tributary superstructure.

For this bridge,

α = 120,000 mm^2

β = 31,400,000 Nmm

γ = 62,800,000 Nmm^2

Then the period of the bridge can be calculated from the expression:

$$T = 2\pi\sqrt{\frac{\gamma}{p_o g \alpha}} \tag{3-6}$$

T = 0.145 sec. for this bridge.

[MCEER/ATC, 2002].

As expected, the period of vibration obtained by using the uniform load method was longer than that obtained using the single mode spectral analysis method, because the uniform load method uses a uniformly distributed load, which is a larger force on the superstructure in the transverse direction of the bridge, compared to the different magnitudes of distributed load along the bridge for the single mode spectral analysis method.

3.14. Design Response Spectrum Curve

After the period of vibration was determined, the next step was to draw the design response spectrum curve, from which the spectral acceleration (S_a) can be obtained. The general shape of a design response spectrum curve is shown in Figure 3.14, which was shown earlier in Chapter 2 as Figure 2.5.

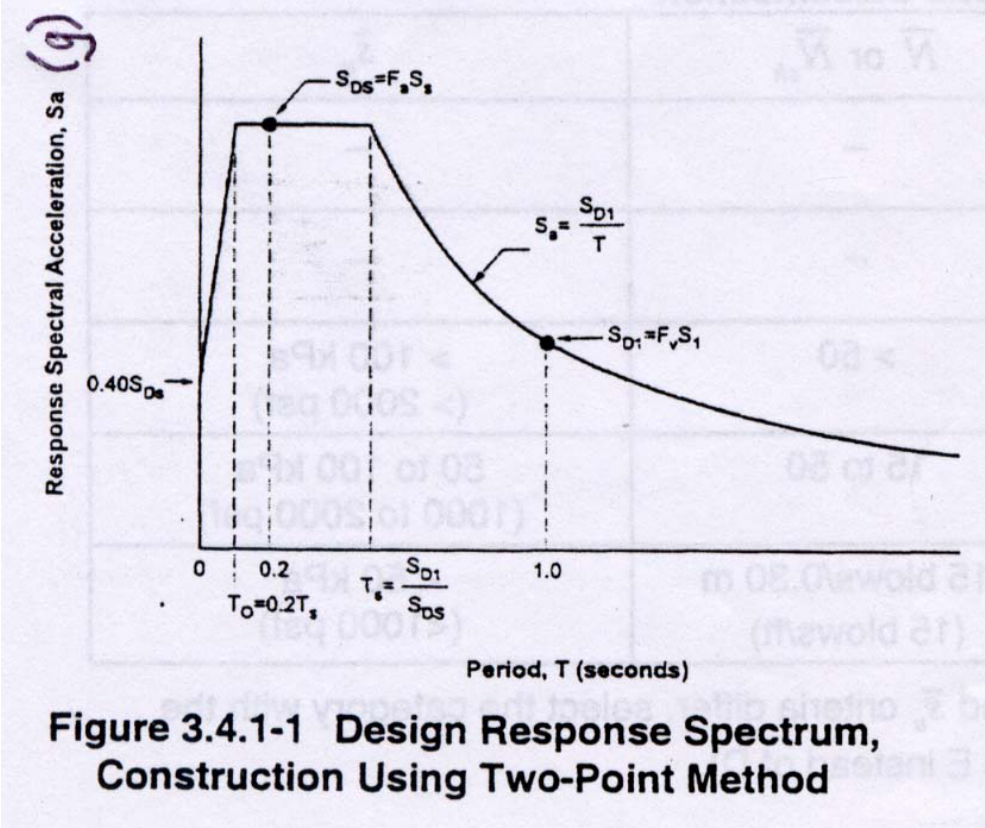

Figure 3.14. The design response spectrum curve in the new LRFD Specifications [MCEER/ATC, 2002].

S_{D1} = 0.0833 g (computed in section 3.9)

S_{DS} = 0.287 g (computed in section 3.9)

$$T_S = \frac{S_{D1}}{S_{DS}} = \frac{0.0833g}{0.287g} = 0.290\,\text{sec}.$$

$T_o = 0.2\ T_s = 0.2$ (0.290 second) = 0.058 second

[MCEER/ATC, 2002].

The design response spectrum curve for this bridge is given in Figure 3.15.

3.15. Equivalent Earthquake Forces

After obtaining the spectral acceleration from the design response spectrum curve, the equivalent earthquake forces could be computed. As for the period of vibration, the equivalent earthquake forces can be computed using the uniform load method and the single mode spectral analysis method [MCEER/ATC, 2002]. Spectral acceleration S_a = 0.287g was the corresponding value for the period of vibration using both methods.

3.15.1. Uniform Load Method

The equivalent earthquake force p_e was calculated using the expression:

$$p_e = \frac{S_a W}{L} \tag{3-7}$$

S_a = the spectral acceleration from the design response spectrum curve [MCEER/ATC, 2002].

For this bridge, p_e = 82.0 N/mm. The complete calculation of the equivalent earthquake force using this method is provided in Appendix VI.

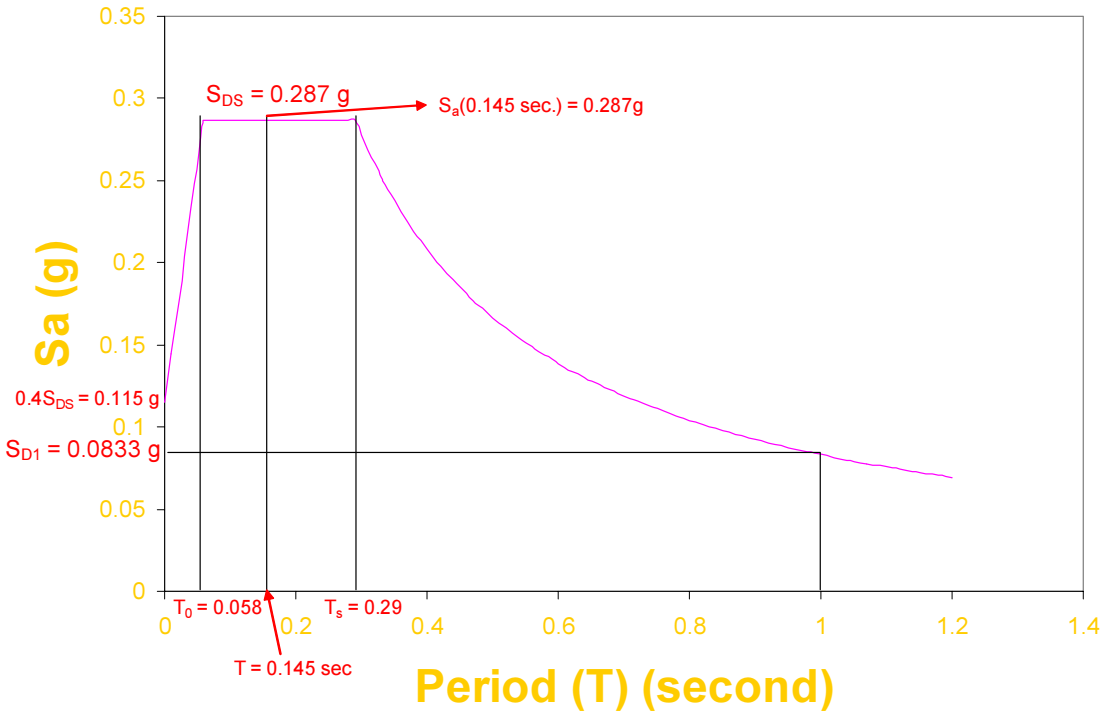

Figure 3.15. The design response spectrum curve for this bridge.

3.15.2. Single Mode Spectral Analysis Method

As explained briefly in section 3.13.2, the equivalent earthquake force computed using this method is not a uniformly distributed load as in the uniform load method. The equivalent earthquake force p_e is calculated using the expression:

$$p_e(x) = \frac{\beta S_a}{\gamma} w(x) v_s(x) \qquad (3\text{-}8)$$

$p_e(x)$ = the equivalent earthquake force for that section

[MCEER/ATC, 2002].

Since each span of the bridge was divided into eleven sections and each section of the span had a different deflection $v_s(x)$, each section also had a different equivalent

earthquake force. Thus the equivalent earthquake loading for the bridge using this method will look like that shown in Figure 3.16. The distributed load in the middle is much larger than the other distributed loads, because the distributed load in the middle carries the tributary load of the substructure. The complete calculation to determine the equivalent earthquake force using this method is presented in Appendix VII.

3.16. Combined Effects of the Dead, Live and Earthquake Loads

The final analysis of the bridge was performed using the cracked section properties for dead, live and earthquake loads. The procedure to calculate the dead and live load effects for this final analysis was the same as when performing the analysis to determine the dead and live load effects to obtain cracked section properties, which was explained earlier in sections 3.6 and 3.7. For the earthquake loads, the axial loads, moments and shears for the pier cap beam and columns were taken directly from the analysis on the entire bridge, unlike the dead and live loads, for which a separate additional analysis was performed on the pier structure. The load factors used to combine the dead, live and earthquake load effects are given in Table 3.4 (Extreme Event-I). But for the earthquake loads, the responses (axial loads, moments and shears) were divided by the R factor given in Table 3.9.

Since SDAP D (Elastic Response Spectrum Method) and the Operational performance level were used in this research study, according to Table 3.9 the earthquake load responses on the columns had to be divided by R=1.5. Thus the combined effects of the dead, live and earthquake loads are given by this expression:

$$P = 1.0DL + 0.5LL + 1.0\left(\frac{EQ}{1.5}\right) \tag{3-9}$$

The complete results of the dead, live and earthquake load effects are given in Appendix VIII.

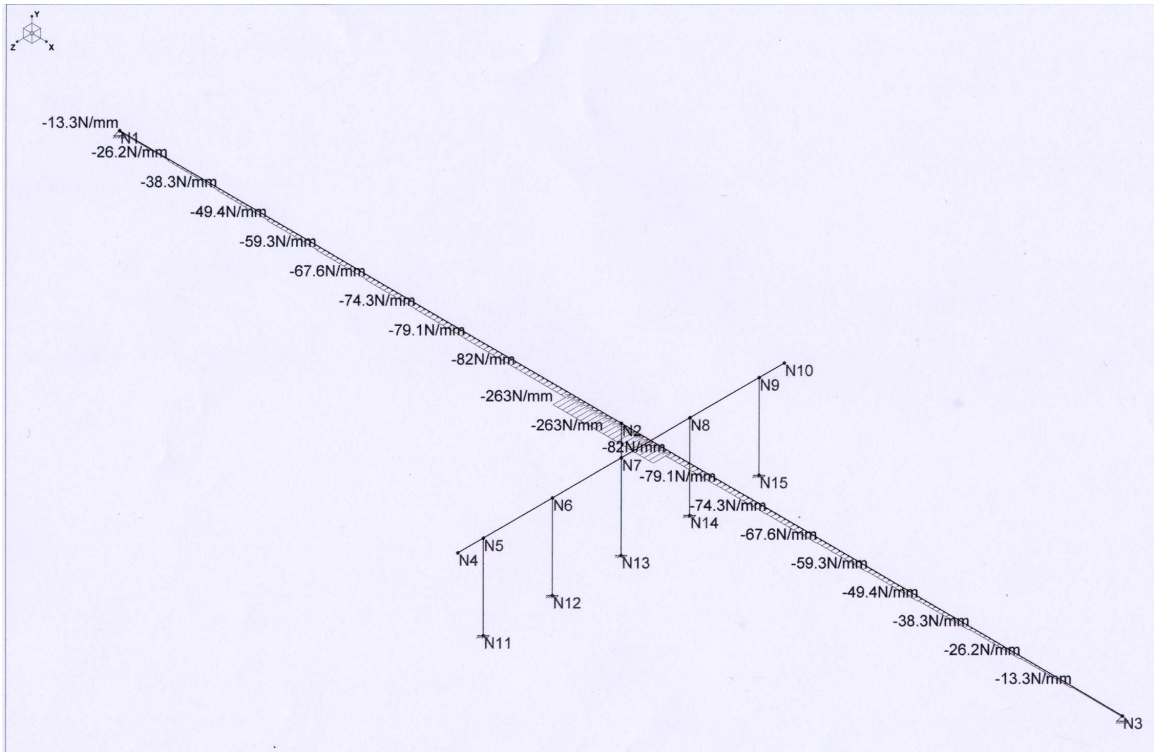

Figure 3.16. The equivalent earthquake loading using the single mode spectral analysis method.

Table 3.9. Base Response Modification Factors, R, for Substructure [MCEER/ATC, 2002].

		Performance	Objective	
	Life	Safety	Operational	
	SDAP	SDAP	SDAP	SDAP
Substructure Element	D	E	D	E
Wall Piers - larger dimension	2	3	1	1.5
Columns - Single and Multiple	4	6	1.5	2.5
Pile Bents and Drilled Shafts -	4	6	1.5	2.5
Vertical Piles - above ground				
Pile Bents and Drilled Shafts - Vertical Piles-2 diameters	1	1.5	1	1
below ground level - No owners approval required.				
Pile Bents and Drilled Shafts - Vertical Piles - in ground -	N/A	2.5	N/A	1.5
Owners approval required.				
Pile Bents with Batter Piles	N/A	2	N/A	1.5
Seismically Isolated Structures	1.5	1.5	1	1.5
Steel Braced Frame - Ductile Components	3	4.5	1	1.5
Steel Braced Frame - Nominally Ductile Components	1.5	2	1	1
All Elements for Expected Earthquake	1.3	1.3	0.9	0.9

3.17. Interaction Diagram of the Columns

The interaction diagram of the columns was constructed to determine if the maximum axial load and moment exceeded the capacity of the column. The complete calculation to determine the important points of the interaction diagram is provided in Appendix IX. For all the columns of this bridge, the maximum axial load and moment were extremely low compared to the capacity of the column, as shown in Figure 3.17. The maximum shear forces in the columns were also far below the shear strength of the columns, as shown in Appendix XI.

3.18. Moment Strength of the Pier Cap Beam

The moment strength of the pier cap beam was calculated to see if or not it was exceeded by the maximum factored moment in the pier cap beam. In order to simplify the calculation of the moment strength, the side reinforcing bars of the pier cap beam were ignored. The actual cross section of the pier cap beam, which was shown earlier in Figure 3.4, was simplified to that shown in Figure 3.18. The complete calculation of the moment strength of the pier cap beam is presented in Appendix X. For the pier cap beam of this bridge,

$\phi M_n = 3.78 \times 10^9$ Nmm

$M_u = 1.66 \times 10^9$ Nmm

$\phi M_n > M_u$

Thus the moment capacity of the pier cap beam was not exceeded.

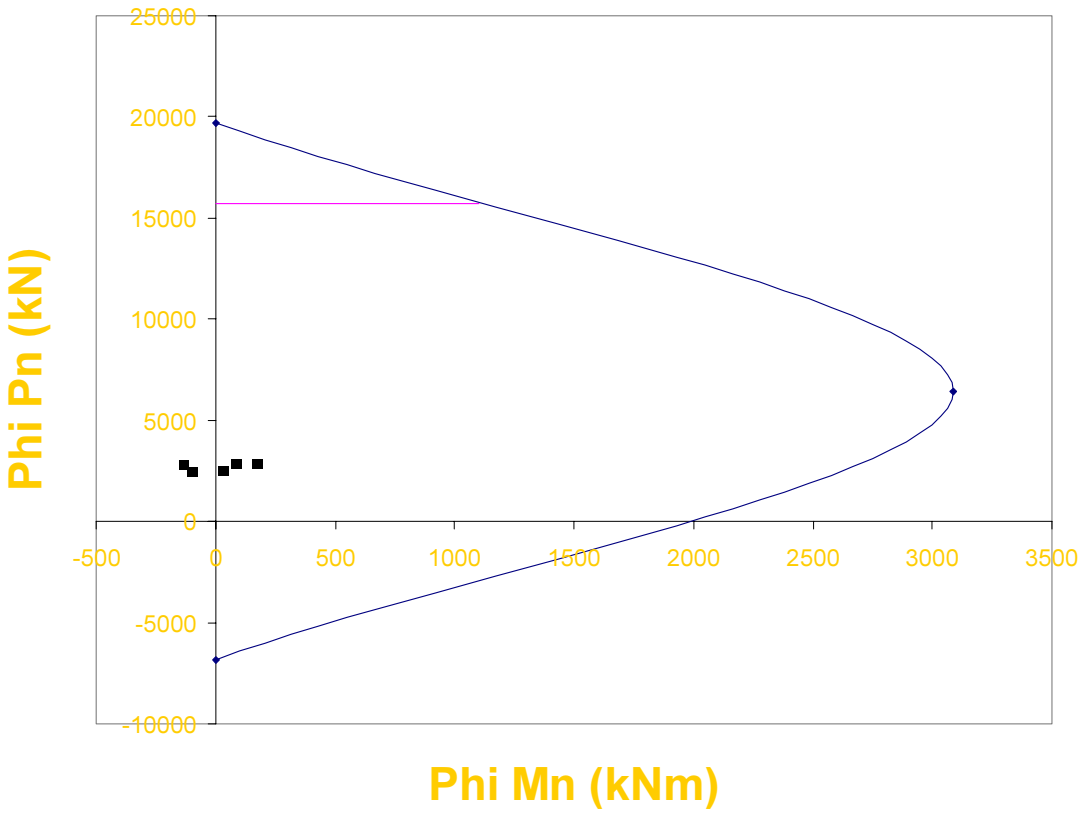

Figure 3.17. The interaction diagram for the columns of the prestressed concrete girder bridge. The black points are the factored axial loads and moments in the columns.

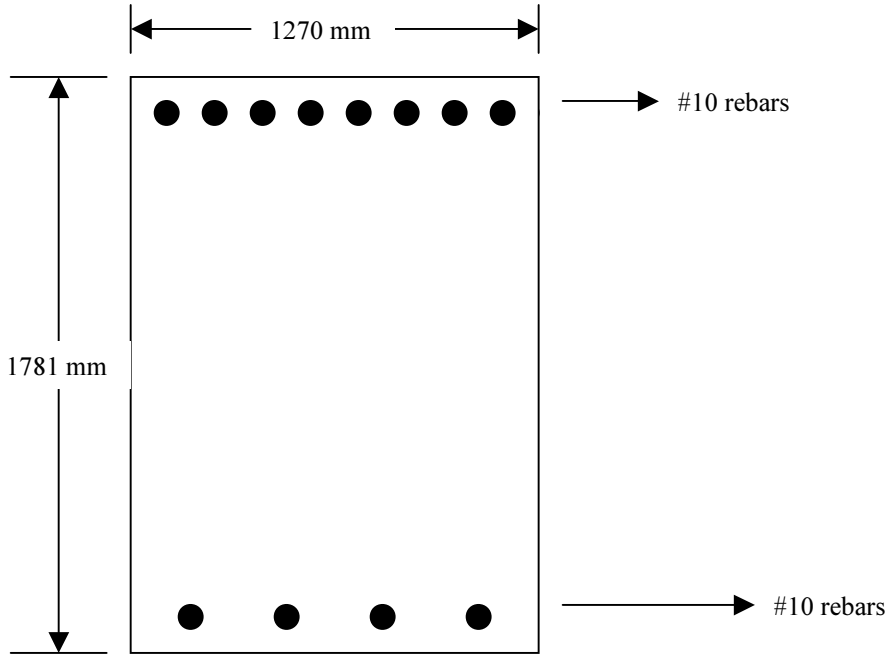

Figure 3.18. The simplified cross section of the pier cap beam.

3.19. Explanation of the Results

The fact that the capacity of the columns is far higher than the maximum axial load and moment in the columns, and the moment strength of the pier cap beam is far above the maximum moment it was subjected to, showed that this bridge was modeled with the substructure much stiffer than the superstructure.

3.20. Detailing Changes due to the New LRFD Guidelines

The details of the bridge must be checked according to the appropriate Seismic Design Requirement, which was SDR 3 for this bridge. The summary of the checks are given in Table 3.10, with the requirements that were not satisfied are shaded.

Table 3.10. The results of the detailing requirement checks for the bridge using Seismic Design Requirement 3.

Number	Requirement	Required	Provided
1a	Transverse Reinforcement Ratio in Potential Plastic Hinge Zones Using the Implicit Shear Detailing Approach	0.00285	0.00362
1b	Transverse Reinforcement Ratio outside the Plastic Hinge Zones Using the Implicit Shear Detailing Approach	0.00160	0.00362
2a	Transverse Reinforcement in Potential Plastic Hinge Zones Using the Explicit Shear Detailing Approach	$V_u - \phi(V_p + V_c) = -490{,}750N$	$\phi V_s = 1{,}480{,}977N$
2b	Transverse Reinforcement outside the Potential Plastic Hinge Zones Using the Explicit Shear Detailing Approach	$V_u - \phi(V_p + V_c) = -855{,}571N$	$\phi V_s = 1{,}480{,}977N$

Number	Requirement	Required	Provided
3	Transverse Reinforcement Ratio for Confinement at Plastic Hinges	0.00687	0.00724
4	Spiral Spacing for Confinement at Plastic Hinges	100 mm	120 mm
5	Transverse Spiral Reinforcement Ratio at the Moment Resisting Connection between the Column and the Pier Cap Beam	0.01481	0.00724
6	Stirrups in the Pier Cap Beam	2,899 mm^2	6,400 mm^2

To bring this bridge up to the new standards, the spiral spacing must be changed from 120 mm to 100 mm, and the spiral size has to be changed from #5 to #7. These changes approximately will result in an additional 0.2% of the total construction cost, which is insignificant. The complete detailing requirements and cost increase calculations are presented in Appendix XI.